IEEE Access
Multidisciplinary | Rapid Review | Open Access Journal

Received May 5, 2020, accepted May 25, 2020, date of publication June 5, 2020, date of current version June 17, 2020.

Digital Object Identifier 10.1109/ACCESS.2020.3000217

Perceiving of Defect Tolerance in Perovskite Absorber Layer for Efficient Perovskite Solar Cell

SAMIYA MAHJABIN[1], MD. MAHFUZUL HAQUE[1], K. SOBAYEL[1], (Associate Member, IEEE), M. S. JAMAL[1,2], M. A. ISLAM[3], (Member, IEEE), V. SELVANATHAN[1], ABDULAZIZ K. ASSAIFAN[4], HAMAD F. ALHARBI[4], K. SOPIAN[1], N. AMIN[5,6], AND MD. AKHTARUZZAMAN[1,6], (Member, IEEE)

[1]Solar Energy Research Institute, The National University of Malaysia, Bangi 43600, Malaysia
[2]Institute of Fuel Research and Development (IFRD), BCSIR, Dhaka 1205, Bangladesh
[3]Department of Electrical Engineering, University of Malaya, Kuala Lumpur 50603, Malaysia
[4]Mechanical Engineering Department, King Saud University, Riyadh 11421, Saudi Arabia
[5]Institute of Sustainable Energy, Universiti Tenaga Nasional (@The National Energy University), Jalan IKRAM-UNITEN, Kajang 43000, Malaysia
[6]Faculty of Engineering and Built Environment, The National University of Malaysia, Bangi 43600, Malaysia

Corresponding authors: K. Sobayel (sobayel@gmail.com) and Md. Akhtaruzzaman (akhtar@ukm.edu.my)

This work was supported in part by The National University of Malaysia under Grant LRGS/1/2019/UKM-UKM/6/1, and in part by the Bangabandhu Fellowship Trust (BBFT), Bangladesh.

ABSTRACT Controlling the defect in the perovskite absorber layer is a very crucial issue for developing highly efficient and stable perovskite solar cells (PSCs) as it exhibits the existence of unavoidable defects even after the careful fabrication process. In this study, the presence of defects in the perovskite layer has been evaluated through the analysis of its structural and optical properties. Then the investigations on the impact of defect density on perovskite absorber layer and its associated solar cell parameters have been carried out by numerical simulation utilizing SCAPS-1D software. Besides the defect density, the thickness of the absorber layer has also been varied to find optimum values of cell parameters. It has been found that when the thickness of absorber and shallow defect density is increased from 200 nm to 800 nm and 1×10^{13} cm^{-3} to 1×10^{18} cm^{-3} respectively, power conversion efficiency (PCE) is varied from 26.7% to 0.90%. However, when the thickness and deep defect density are raised from 200 nm to 800 nm and 1×10^{13} cm^{-3} to 1×10^{16} cm^{-3}, respectively, the PCE is varied from 19.3% to 6.15%. It is revealed that optimum absorber thickness is 550 nm and the tolerances of shallow level and deep level defect density are 1×10^{17} cm^{-3} and 1×10^{15} cm^{-3}, respectively.

INDEX TERMS Perovskite, defect tolerance, shallow level defect, deep level defect, SCAPS-1D.

I. INTRODUCTION

Perovskite solar cells (PSCs), which include perovskite structured compound as a light absorber layer, have quickly appeared as the most favorable photovoltaic technology. It is because of the noble electrical and physical properties of perovskite such as direct (1.5 eV) and tunable bandgap (1.2 eV to 3.17 eV), low exciton binding energy (∼20 meV) at room temperature [1]–[3], high bipolar conductivity (10^{-2} – 10^{-3} Scm^{-1}), high carrier mobility (∼20 cm^{2}V^{-1}s^{-1}) [4], [5], high absorption coefficient (1.5×10^4 cm^{-1} at 550 nm), long electron-hole diffusion length (more than 175 μm for $CH_3NH_3PbI_3$ and more than 380 μm for $CH_3NH_3PbI_{3-x}Cl_x$), high charge carrier lifetime (>15 μs), easy solution processability, competitive cost and sufficient availability on earth [6]–[8].

Despte the immense advantages of perovskite absorber layers, the presence of defects plays a negative role in the cell performance as these defects create hysteresis [9], non-radiative recombination [10], charges trapping [11], charges scattering [12], ion-migration [13] in PSCs.

These defects are responsible for limiting the power conversion efficiency (PCE) of PSCs up to 25.2%, far below the thermodynamic PCE limit of ∼31% for $MAPbI_3$ [14]. Moreover, these defects also noticeably affect the long-term stability of PSCs [15]. Therefore, it is highly desirable to

The associate editor coordinating the review of this manuscript and approving it for publication was Giambattista Gruosso.

develop high-performance PSCs with efficient control of the defects in the perovskite absorber layer.

Since it is a great challenge to develop a defect-free perovskite layer, the initial aim of this research was to propose a careful procedure of preparing a perovskite film with zero defect or less defect. But PL spectroscopy of the developed film has shown the presence of the defect. Then it has been planned to execute the research in two steps. The first step identifies the presence of defects in perovskite absorber layer by experimental methods that validate the literature of this study and the second step evaluates the impact of both shallow level and deep level defect on PCE and some other cell parameters of PSCs by numerical simulation. Besides, the effects of the absorber layer's thickness variation have also been discussed. In this study, SCAPS-1D has been used to study cell performances and to provide guidance for designing efficient PSCs.

II. DEFECTS AT PEROVSKITE LAYER

A. SHALLOW LEVEL DEFECT & DEEP LEVEL DEFECT

As metal halide perovskites show high radiative efficiency, PSCs have better power conversion efficiency than many other kinds of solar cells such as dye-sensitized solar cells, organic solar cells, cadmium telluride solar cells, etc. [14]–[16]. Despite this remarkable property, when perovskites are interfaced into devices, they face a higher non-radiative loss than inorganic materials like gallium arsenide [17]. This occurs due to the defects in the perovskite absorber layer. These defects appear as point defects such as atomic vacancies, interstitials, and anti-site substitutions or higher dimensional defects such as dislocations, grain boundaries, and precipitates [18]. The creation of single point defects by environmental conditions associated with the regular properties of the crystal structure of the semiconductor. Moreover, the formation energy of point defects also depends on the conditions of the film fabrication process such as precursor concentrations, precursor ratio, solvents, temperature, and doping, etc. which can be expressed by the following equation (1) [19].

$$E_f = E_v - E_{sc} + \mu_c \tag{1}$$

where, E_v and E_{sc} are the total energy of the vacancy defect system and defect-free super cell structure, respectively. μ_c is the chemical potential of lead iodide (PbI_2) or methyl ammonium iodide (MAI). To attract trap-free carriers, the presence of a point defect could generate a carrier recombination center within the semiconductor bandgap which will form shallow or deep electron transition levels in the forbidden region [20]. Shallow transition energy level (STEL) is formed if point defect possesses the lowest formation energy [19], [21]–[26]. This defect trap exists near the conduction band minimum (CBM) or valance band maximum (VBM), which gives more chance to the trapped carrier for detrapping. Moreover, in STEL, the charge recombination rate is low, which stimulates the carrier mobility and enhances photovoltaic efficiency [20].

On the other hand, the deep defects trap (DDT) in perovskite prevents the PCE of PSCs to reach the Schockley-Queisser limit [27]. The deep transition energy level is formed if point defects possess the highest formation energy [19], [21]–[26]. It is also known as the Shockley-Read-Hall recombination center. Due to this recombination center, the trapped carrier annihilates or recombines with an opposite carrier before it can be emitted. This incident intensely reduces the quantum efficiency of photoluminescence and photovoltaic efficiency of solar cells. The Shockley- Read- Hall recombination is expressed in equation (2) [28]–[30].

$$R^{SRH} = \frac{\vartheta \sigma_n \sigma_p N_T \left(np - n_i^2\right)}{\sigma_p \left(p + p_1\right) + \sigma_n \left(n + n_1\right)} \tag{2}$$

where σ_n and σ_p are capture cross-sections for electrons and holes respectively, is electron thermal velocity, N_T is defect density, n_i is intrinsic number density, n and p are the concentrations of electrons and holes respectively at equilibrium, n_1 and p_1 are the concentrations of electrons and holes in trap defect and valance band, respectively. R^{SRH} is directly proportional to the defect density of the perovskite absorber layer. Moreover, charge diffusion length, carrier lifetime, steady-state electron/hole density are decreased due to the presence of DDT. The relation between diffusion length, carrier mobility, and lifetime is expressed in equation (3) [31].

$$L = \sqrt{\frac{\mu\,(e,h)\,RT}{q}\tau_{lifetime}} \tag{3}$$

Here, L, μ (e, h), and $\tau_{lifetime}$ are the diffusion length, the electron and hole mobility, and the minority carrier lifetime, respectively. Meanwhile, $\tau_{lifetime}$ depends upon the defect trap density and capture cross-section area for electrons and holes. The relation between $\tau_{lifetime}$ and bulk defect density is expressed in equation (4) [31].

$$\tau_{lifetime} = \frac{1}{N_T \sigma v_{th}} \tag{4}$$

Here σ, v_{th} and N_T represent the capture cross-section area for electrons and holes, the thermal velocity of carriers, and defect density, respectively. Higher-dimensional defects such as grain boundaries and surface traps are considered to be composed of deep-level defects and thus are significantly liable for the non-radiative recombination process.

B. IDENTIFICATION OF DEFECTS

Defect states and their spatial locations have been identified through some characterization methods in several types of research. To date, measurements of time-integrated photoluminescence (PL) [32], [33], time-resolved PL [32]–[34], microwave conductivity, and femtosecond transient absorption [35] have found and estimated the densities of bulk defect states in the perovskite layer. Femtosecond transient absorption microscopy (TAM) and time-integrated photoluminescence (PL) microscopy are optical, contactless,

and noninvasive methods that quantify the spatial distributions of electronic excited-states and map the emission propensity at the exact same spatial locations in the sample [36]. Also, confocal fluorescence microscopy associated with scanning electron microscopy demonstrates the local fluorescence lifetime imaging that offers a path through which perovskite layer processing modifications can be studied to evaluate their effects on this layer carrier recombination [37]. Ultraviolet photoemission spectroscopy (UPS) technique is used to probe the preferential trapping of charge carriers on perovskite surfaces [35]. Moreover, the origin of the radiative recombination center of photoexcited charges in the perovskite layer is investigated by scanning near-field optical microscopy and atomic force microscopy (AFM) [38]. Beside these effective experimental characterization techniques, the most popular and versatile computational quantum mechanical modeling method named density functional theory (DFT) is used to investigate perovskites' defects properties theoretically [39].

Nowadays it is a matter of great success that, some techniques, such as passivation approach (chemical surface treatments), production of light-soaking films, etc. are used to reduce the non-radiative loss in perovskite films [15]. Though these processes lead toward defect-free materials, still the defects in perovskite layers are unavoidable in any circumstance.

III. METHODOLOGY

A. EXPERIMENTAL DESIGN AND PROCEDURE

Aiming to develop a defect less perovskite absorber layer, at first the halide perovskite ($CH_3NH_3PbI_3$) precursor solution for spin-coating was prepared by mixing MAI (0.241 g) with PbI_2 (0.084 g), maintaining a molar ratio of 3:1, in anhydrous *N, N*-dimethylformamide (DMF) (326 μl). Then 81.5 μl Dimethyl sulfoxide (DMSO) was added to this solution. That solution was stirred at 800 rpm for 60 minutes at 65^0 C to produce a perovskite solution. After that, the perovskite solution was spin-coated onto pre-cleaned glass substrates at 6000 rpm for 30 seconds. Finally, the samples were thermally annealed at 100^0 C for 60 minutes in an N_2-filled glovebox to form perovskite films.

B. CHARACTERIZATION

Structural and crystalline properties of the as-grown films were examined by the BRUKER AXS-D8 ADVANCE X-ray diffractometer at room temperature. X-ray diffraction (XRD) patterns were recorded in the 2θ range of 10^0 to 40^0 with a step size of 0.05^0 using Cu Kα radiation wavelength, $\lambda = 0.15408$ nm. Grain size, surface morphology, and cross-sectional view were observed by using Carl Zeiss Merlin field emission scanning electron microscope (FESEM) operated at 3 kV. PL spectroscopy is performed to analyze defects in the developed metal halide perovskite films, as it is a useful characterization method for identifying the defects in semiconductors. PL measurements were carried out on

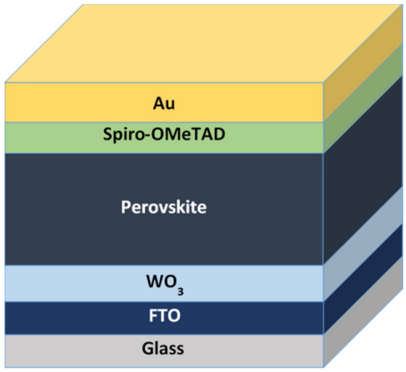

FIGURE 1. Schematic diagram of a planar structure of PSC.

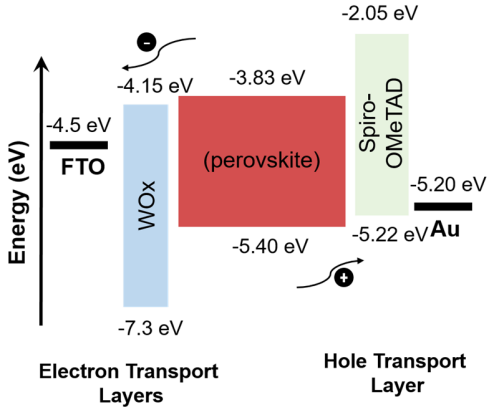

FIGURE 2. Relative energy band diagram of different layers in PSC.

an FLS 920 (Edinburgh Instruments Ltd.) fluorescence spectrometer in which 450-watt xenon lamp was used as the excitation source at room temperature. The developed perovskite film was excited by the light of 500 nm wavelength, elected by the excitation monochromator. Finally, the luminescence from the film was detected by a photo multiplier tube after passing through an emission monochromator.

C. NUMERICAL SIMULATION

Different kinds of structures of PSCs have been explored to date, such as mesoporous, planar, and inverted planar architectures. The planar architecture has been planned to be studied using numerical simulation, where the metal halide perovskite absorber layer is the most dominating part of the PCE of the cell. In this study, the planar architecture as FTO/WO_3/$CH_3NH_3PbI_3$/Spiro-OMeTAD/Au has been considered, which is shown in figure 1 and its energy level diagram [40] is shown in figure 2. According to figure 1, the perovskite absorber layer is sandwiched between electron transport layer (ETL), made of WO_3 and hole transport layer (HTL), made of Spiro-OMeTAD, whereas the fluorine doped tin oxide (FTO) and gold (Au) are used as a transparent front contact and top metal back contact, correspondingly. Though TiO_2 has been being used widely as ETL, it has not been chosen in the proposed solar cell because of its low electron mobility, which causes the reduction in cell

TABLE 1. Selected parameters for numerical simulation.

Parameters and units	WO_3	$CH_3NH_3PbI_3$	Spiro-OMeTAD
Bandgap (eV)	3.15	1.57	3.17 [40]
Electron Affinity (eV)	4.55	3.9 [42]	2.45 [48]
Dielectric Permittivity (relative)	10	10 [43]	3 [48]
Effective Conduction Band Density (cm^{-3})	4.2×10^{18}	2.75×10^{18} [44]	2.2×10^{18} [48]
Effective Valence Band Density (cm^{-3})	9×10^{18}	3.9×10^{18} [44]	1.9×10^{19} [48]
Electron and Hole thermal velocity (cm/s)	1×10^{7}	1×10^{7}	1×10^{-7} [48]
Electron Mobility (cm^2/Vs)	20 [41]	10 [45]	2×10^{-4} [48]
Hole Mobility (cm^2/Vs)	10	10 [45]	2×10^{-4} [48]
Acceptor Concentration (cm^{-3})	0	1×10^{9} [46]	1×10^{18}
Donor Concentration (cm^{-3})	2×10^{18} [49]	1×10^{9} [46]	0
Capture Cross Section for Electrons (cm^2)	1×10^{-15}	1×10^{-12}	1×10^{-12}
Capture Cross Section for Holes (cm^2)	1×10^{-15}	1×10^{-15}	1×10^{-15}

efficiency as a result of charge accumulation at the interface of ETL and perovskite. Here WO_3 is considered as the ETL for its high electron mobility (10-20 $cm^2V^{-1}s^{-1}$), which results in efficient transportation of photogenerated electron. Besides, WO_3 is chemically stable in a corrosive environment [41].

Table 1 shows the simulation parameters, which are summarized from various reported works [40]–[49]. The parameters were chosen based on literature to make sure that the obtained results from the simulation baseline have the proper indication of a real-world scenario.

IV. RESULTS AND DISCUSSION

A. FILM MORPHOLOGY

It is revealed that as-deposited film exhibits crystalline properties by the ocular study. Intermolecular bond and layered structure have been found compact through FESEM image.

Figure 3(a) shows a top view, and 3(b) shows the cross-sectional FESEM image of the as-grown perovskite layer. The film shows compact irregular granular morphology and reveals dense microstructure. The grain size has been measured by image-J software, and the average grain size has been found 114.08 nm.

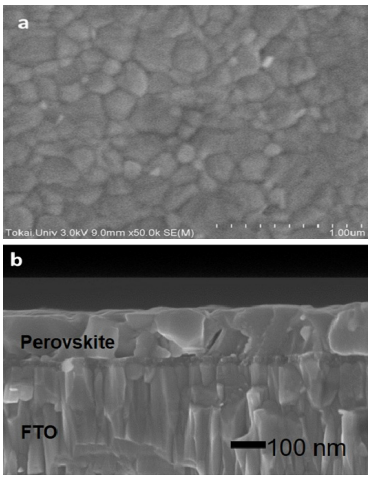

FIGURE 3. Perovskite film morphology (a) top view and (b) cross-sectional image.

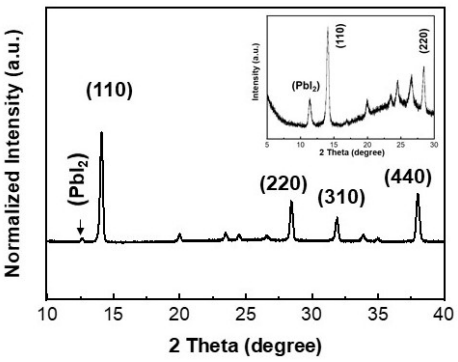

FIGURE 4. XRD peak of as-deposited perovskite layer (Inset shows the XRD patterns of a degraded perovskite film).

B. EVALUATING DEFECTS FROM STRUCTURAL PROPERTIES

Figure 4 shows the XRD patterns of the perovskite film deposited on FTO-substrate, where 2θ angle ranged from 10^0 to 40^0. The diffraction peaks were detected at 2θ angles of 14.1^0, and 28.4^0 in perovskite film, where the peaks were assigned to the (110), and (220) crystal planes, respectively. These intense high peaks indicate the formation of perovskite's tetragonal phase [60]. Though the stronger and sharper diffraction peak at $2\theta = 14.1^0$ proves the high crystallinity of perovskite, a weak peak was observed around 12.7^0, which corresponds to the unconverted PbI_2.

Additionally, inset in figure 4 shows the degraded perovskite on FTO-substrate. An additional peak at 2θ angle of 12.48^0 has been observed which leads to PbI_2. This intense PbI_2 peak implies the presence of defect or degradation of the perovskite layer or ion mitigation or process limitations [50]. The β value has been observed 0.38^0 which is quite high in comparison to the reported value of 0.1^0 [50]. Higher β value represents the deterioration of film's crystalline properties [51]. Thus, it confirms the presence of defects in the fabricated sample.

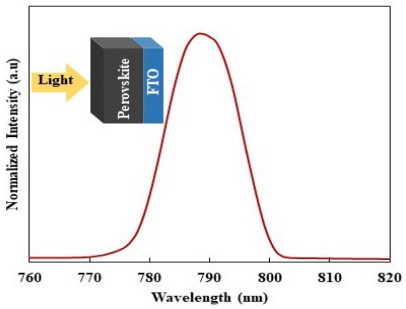

FIGURE 5. PL Spectroscopy for the developed perovskite absorber layer.

The average particle size or crystallite size has been calculated from the broadening of the (110) peak using Scherrer's equation (5) [52].

$$L\,(hkl) = \frac{0.9\lambda}{ß\cos\theta} \tag{5}$$

where L, λ, ß, and θ are the crystallite size, wavelength, FWHM, and the angle between the incident and scattering planes, respectively. Crystalline size has been calculated and ranges from 210.2 Å to 284.1 Å. Crystallinity percentage has been achieved to 72% from XRD analysis. Grains with different relative orientations and positions create the difference in phase variations when a light wave is scattered by them. A large number of grains with different orientations create displacement of the atom while forming crystal lattice [51]. The lattice strains exhibit displacement of atoms from their original lattice positions. This displacement in crystal lattice creates defects or traps in the film. Moreover, the lower value of strain signifies higher crystallinity [33]. The strain has been calculated by the following relation of equation (6) [53].

$$\varepsilon = \frac{\beta}{4tan\theta} \tag{6}$$

Here, ε is the strain. The strain value has been calculated and found at 14.62×10^{-3}. Dislocation density (δ) is another important factor for determining the crystallographic properties of the thin film. Dislocation is caused by the imperfections in crystal orientation. It is measured by Williamson and Smallman's relations equation (7) [54].

$$\delta = \frac{1}{L^2} \tag{7}$$

Here, δ is the dislocation density, and L is crystallite size. The δ value has been obtained at 2.26×10^{-3} nm^{-2} (max). From the structural analysis, it is evident that the fabricated film has various types of defects in its crystalline structure.

C. EXAMINING OF DEFECTS FROM OPTICAL PROPERTIES

From the study of PL spectroscopy shown in figure 5, emission peak is found around 788 nm wavelength of light, equivalent to 1.57 eV photon energy representing the bandgap (E_g) of the developed lead iodide perovskite thin films, which is a fairly good agreement with the reported band gap values of metal halide perovskites [1].

Though a sharp peak is expected for the defect less semiconductor, a significant amount of line broadening is observed in PL spectroscopic image. Line broadening Γ(T) can be expressed as equation (8), which is the sum over the various contributions [55]–[57].

$$\Gamma(T) = \Gamma_0 = \Gamma_{ac} + \Gamma_{LO} + \Gamma_{imp} \tag{8}$$

Here, Γ_0 represents temperature-independent inhomogeneous broadening, which is the effect of scattering due to imperfections and disorder [55], [56], [58]. The second and third terms (Γ_{ac} and Γ_{LO}) represent homogeneous broadening, which is found to form acoustic and LO phonon (Fröhlich) scattering, respectively [55], [56], [58], [59]. The final term, Γ_{imp}, phenomenological accounts for scattering from ionized impurities [55], [56].

Since defects are nothing but the imperfections, it can be mentioned that all types of defects are also the reasons behind the Γ_0 term in line broadening of equation 8. So, defects play an important role behind the reason for line broadening in PL spectroscopy along with different types of phonon scatterings. The existence of several types of defects in the developed perovskite absorber layer suggests developing the layer more carefully for avoiding defects. However, it seems to be extremely challenging to produce defect less film. So, before further developing the absorber layer with zero defects or fewer defects, it is planned to analyze the dependency level of solar cell efficiency on the defects in the perovskite layer. Among various types of defects, shallow level defects, and deep level defects are focused on analyzing their effects on the solar cell parameters using numerical simulation.

D. IMPACT OF SHALLOW DEFECT TRAP

The impact of the shallow defect trap (SDT) has been investigated by numerical simulation. In this study density of defect has been varied from 10^{13} to 10^{18} cm^{-3} while its impact on planar PSC has been recorded and depicted in figure 6.

The thickness of the absorber layer of perovskite is needed to be optimized to get the best photovoltaic performances of a solar cell. This layer must be sufficiently thick enough to take full advantage of light absorption. Again, too much thick absorber layer can increase electron-hole recombination, which may reduce efficiency. Thus, it is needed to be thin as well to the proficient collection of photogenerated carriers.

Figure 6a depicts the variation of power conversion efficiency η with respect to absorber layer thickness and defect density. The thickness of the perovskite layer has been varied from 200 nm to 800 nm. Efficiency has been increased with the increment of thickness. Here observed highest efficiency is 26.7% for the thickness of 800 nm. However, it has been found that when thickness increases from 550 nm to 800 nm; there was a nominal increment of efficiency. Thus, the optimized thickness of the perovskite layer can be considered 550 nm, which provides an efficiency of 24.32%. From the same figure, it has been revealed that the η varies from 26.7% to 0.90% for the variation of defect density from 1×10^{13} cm^{-3} to 1×10^{18} cm^{-3} when the thickness varies

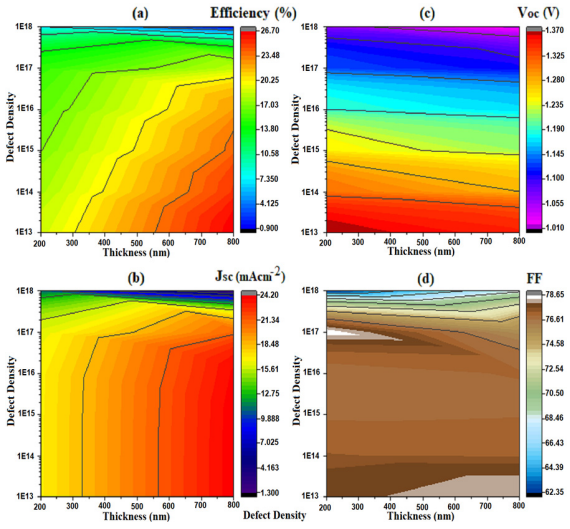

FIGURE 6. Impact of shallow defect trap. (a) Impact on power conversion efficiency (η), (b) Impact on short circuit current density (J_S), (c) Impact on open-circuit voltage (V_O) and (d) Impact on fill factor (FF).

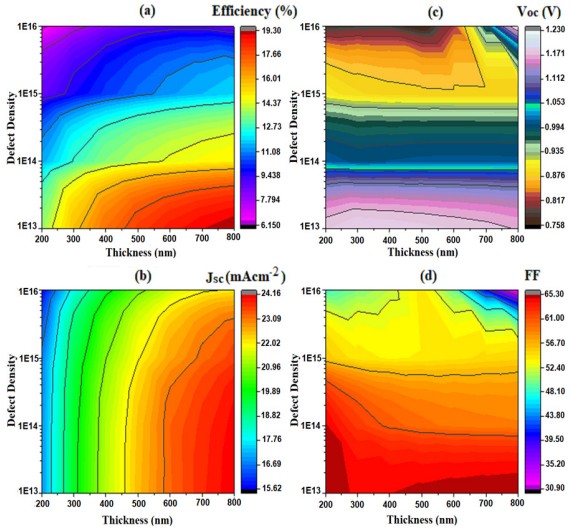

FIGURE 7. Impact of deep defect trap. (a) Impact on power conversion efficiency (η), (b) Impact on short circuit current density (J_S) (c) Impact on open-circuit voltage (V_O), and (d) Impact on fill factor (FF).

from 200 nm to 800 nm. The best photovoltaic η is obtained by 26.7% for the defect density of $1 \times 10^{13}\text{cm}^{-3}$.

As shown in figure 6b, the short circuit current density J_{sc} decreases from 24.20 mAcm^{-2} to 1.3 mAcm^{-2} when the defect density of the perovskite absorber layer increases from 1×10^{13} cm^{-3} to 1×10^{18} cm^{-3}. The open-circuit voltage (V_{oc}), originated from the energy difference between the photo-excited free electrons and holes [20], reduces from 1.37 V to 1.0 V (figure 6c) and the fill factor (FF) decreases from 78.65% to 62.35% (figure 6d) when the defect density of perovskite absorber layer increases from 1×10^{13} cm^{-3} to $1 \times 10^{18}\text{cm}^{-3}$. In this study, when the defect density is varied from 1×10^{17} cm^{-3} to 1×10^{18} cm^{-3} at 550 nm thickness, the efficiency η is degraded drastically from 18.4% to 0.90%. So, the tolerance of defect density is up to 1×10^{17} cm^{-3}. In the case of $MAPbI_3$, despite the detrapping of charges captured by SDT, the recombination rate can be very high without compromising the performance of PSCs. This is because the emitted photons would probably be reabsorbed by the perovskite. As expected, the photons get ''recycled'' before charge extraction by the respective electrodes. Moreover, the charge diffusion length of $MAPbI_3$ is reported covering a large range from several hundreds of nanometers to micrometers. This demonstrates that, as long as the free charge is not trapped and non-radiatively recombined via deep-level defects, it can be fully extracted from the perovskite and yield high PCE [20]. So, the presence of SDT is not a major problem for perovskite.

E. IMPACT OF DEEP DEFECT TRAP

The impact of deep defect trap (DDT) is discussed with the assistance of figure 7. The position of deep transition energy level is in the middle of the forbidden energy gap of the perovskite layer. For the variation of deep defect density from 1×10^{13} cm^{-3} to $1 \times 10^{16}\,\text{cm}^{-3}$ and the absorber layer thickness from 200 nm to 800 nm, the efficiency η varies from 19.30% to 6.15% (figure 7a). The best photovoltaic efficiency η is 19.30%, which has been found for the defect density of $1 \times 10^{13}\text{cm}^{-3}$. It is observed that the efficiency η decrease with the increasing value of defects density in the perovskite layer.

As shown in figure 7b, the J_{sc} slowly decreases from 24.16 mA/cm^2 to 15.62 mA/cm^2 when the deep defect density of the perovskite layer increases from 1×10^{13} cm^{-3} to $1 \times 10^{16}\text{cm}^{-3}$. The V_{oc} reduces gradually from 1.23 V to 0.75 V when the defect density increases from 1×10^{13} cm^{-3} to 1×10^{16} cm^{-3} as shown in figure 7c. The decrement of V_{oc} and J_{sc} is due to the recombination of the carrier with the localized energy level. Fill factor (FF) value decreases from 65.30% to 30.90% with the increment of defect density (figure 7d). In this investigation, when deep defect density increases from 1×10^{14} cm^{-3} and above, the efficiency η drastically reduces from 16.01% to 6.15%. Thus, the tolerance of defect density for the deep level defect is lower than the shallow level defect, and it is up to 1×10^{15} cm^{-3}.

V. CONCLUSION

This study evaluates the presence of defects in the perovskite layer by a thorough investigation of its structural and optical properties. By studying its structural properties, an inadmissible peak has been observed from its XRD graph, which affirms the presence of defects in the film. Again, line broadening in PL spectroscopy of the carefully developed film proves the presence of defects as well. Among different types of defects in the perovskite absorber layer, the SDT and DDT both have detrimental effects on the PSCs performances. These effects have been clearly realized

from the simulation results, conducted by the SCAPS-1D for PSCs considering the architecture FTO/WO_3/$CH_3NH_3PbI_3$/Spiro-OMeTAD/Au.

Simulation results show that, when shallow level defect density in the perovskite absorber layer is increased from 1×10^{13} cm^{-3} to 1×10^{18} cm^{-3}, the PCE decreases from 26.7% to 0.9%. For deep level defects, PCE decreases from 19.30% to 6.15% due to the increment of deep defect density from 1×10^{13} cm^{-3} to $1 \times 10^{16} cm^{-3}$ in the perovskite absorber layer. The optimum absorber thickness has been found 550 nm while the tolerances of density of shallow level and deep level defect have been found $1 \times 10^{17} cm^3$ and $1 \times 10^{15} cm^{-3}$ respectively. Therefore, the photovoltaic efficiency of perovskite solar cells reduces more for deep level defects compared to shallow level defects. Through these simulation results it is clear that, if the perovskite absorber layer of proposed thickness is developed within these tolerance levels of defects, it can be used in developing the complete solar cell for getting higher cell efficiency.

ACKNOWLEDGMENT

The authors thankfully acknowledge Dr. Marc Bargeman, Ghent University, Belgium, for providing the SCAPS-1D simulation software and research assistance, and Dr. Shahiduzzaman, Nanomaterials Research Institute (NanoMaRi), Kanazawa University, Japan, for his contribution on conducting research during the period of COVID-19.

REFERENCES

[1] A. Kojima, K. Teshima, Y. Shirai, and T. Miyasaka, "Organometal halide perovskites as visible-light sensitizers for photovoltaic cells," *J. Amer. Chem. Soc.*, vol. 131, no. 17, pp. 6050–6051, May 2009.

[2] J. Jeng, Y. F. Chiang, M. H. Lee, S. R. Peng, T. F. Guo, P. Chen, and T. C. Wen, "Methylammonium lead iodide perovskite/fullerene-based hybrid solar cells," *SPIE Newsroom*, vol. 10, no. 2, 2014, Art. no. 005033.

[3] A. Toshniwal, A. Jariwala, V. Kheraj, A. S. Opanasyuk, and C. J. Panchal, "Numerical simulation of tin based perovskite solar cell: Effects of absorber parameters and hole transport materials," *J. Nano Electron. Phys.*, vol. 9, no. 3, pp. 1–4, 2017.

[4] V. D'Innocenzo, G. Grancini, M. J. P. Alcocer, A. R. S. Kandada, S. D. Stranks, M. M. Lee, G. Lanzani, H. J. Snaith, and A. Petrozza, "Excitons versus free charges in organo-lead tri-halide perovskites," *Nature Commun.*, vol. 5, no. 1, p. 3586, May 2014.

[5] C. C. Stoumpos, C. D. Malliakas, and M. G. Kanatzidis, "Semiconducting tin and lead iodide perovskites with organic cations: Phase transitions, high mobilities, and near-infrared photoluminescent properties," *Inorganic Chem.*, vol. 52, no. 15, pp. 9019–9038, Aug. 2013.

[6] H. Oga, A. Saeki, Y. Ogomi, S. Hayase, and S. Seki, "Improved understanding of the electronic and energetic landscapes of perovskite solar cells: High local charge carrier mobility, reduced recombination, and extremely shallow traps," *J. Amer. Chem. Soc.*, vol. 136, no. 39, pp. 13818–13825, Oct. 2014.

[7] M. Acik and S. B. Darling, "Graphene in perovskite solar cells: Device design, characterization and implementation," *J. Mater. Chem. A*, vol. 4, no. 17, pp. 6185–6235, 2016.

[8] F. Zhang, B. Yang, Y. Li, W. Deng, and R. He, "Extra long electron–hole diffusion lengths in $CH_3NH_3PbI_{3-x}Cl_x$ perovskite single crystals," *J. Mater. Chem. C*, vol. 5, no. 33, pp. 8431–8435, 2017.

[9] E. M. Hutter, G. E. Eperon, S. D. Stranks, and T. J. Savenije, "Charge carriers in planar and meso-structured organic–inorganic perovskites: Mobilities, lifetimes, and concentrations of trap states," *J. Phys. Chem. Lett.*, vol. 6, no. 15, pp. 3082–3090, Aug. 2015.

[10] H.-S. Kim, C.-R. Lee, J.-H. Im, K.-B. Lee, T. Moehl, A. Marchioro, S.-J. Moon, R. Humphry-Baker, J.-H. Yum, J. E. Moser, M. Grätzel, and N.-G. Park, "Lead iodide perovskite sensitized all-solid-state submicron thin film mesoscopic solar cell with efficiency exceeding 9%," *Sci. Rep.*, vol. 2, no. 1, Dec. 2012, Art. no. 591.

[11] M. M. Lee, J. Teuscher, T. Miyasaka, T. N. Murakami, and H. J. Snaith, "Efficient hybrid solar cells based on meso-superstructured organometal halide perovskites," *Science*, vol. 338, no. 6107, pp. 643–647, Nov. 2012.

[12] W. S. Yang, B.-W. Park, E. H. Jung, N. J. Jeon, Y. C. Kim, D. U. Lee, S. S. Shin, J. Seo, E. K. Kim, J. H. Noh, and S. I. Seok, "Iodide management in formamidinium-lead-halide–based perovskite layers for efficient solar cells," *Science*, vol. 356, no. 6345, pp. 1376–1379, 2017.

[13] W. E. I. Sha, X. Ren, L. Chen, and W. C. H. Choy, "The efficiency limit of $CH_3NH_3PbI_3$ perovskite solar cells," *Appl. Phys. Lett.*, vol. 106, no. 22, Jun. 2015, Art. no. 221104.

[14] T. C. Sum and N. Mathews, "Advancements in perovskite solar cells: Photophysics behind the photovoltaics," *Energy Environ. Sci.*, vol. 7, no. 8, pp. 2518–2534, 2014.

[15] H. J. Snaith, "Perovskites: The emergence of a new era for low-cost, high-efficiency solar cells," *J. Phys. Chem. Lett.*, vol. 4, no. 21, pp. 3623–3630, Nov. 2013.

[16] H. S. Jung and N.-G. Park, "Perovskite solar cells: From materials to devices," *Small*, vol. 11, no. 1, pp. 10–25, Jan. 2015.

[17] J. M. Ball and A. Petrozza, "Defects in perovskite-halides and their effects in solar cells," *Nature Energy*, vol. 1, no. 11, p. 16149, Nov. 2016.

[18] H.-S. Duan, H. Zhou, Q. Chen, P. Sun, S. Luo, T.-B. Song, B. Bob, and Y. Yang, "The identification and characterization of defect states in hybrid organic–inorganic perovskite photovoltaics," *Phys. Chem. Chem. Phys.*, vol. 17, no. 1, pp. 112–116, 2015.

[19] Z. Xiao, Y. Yuan, Y. Shao, Q. Wang, Q. Dong, C. Bi, P. Sharma, and A. Gruverman, "Giant switchable photovoltaic effect in organometal trihalide perovskite devices," *Nature Mater.*, vol. 14, no. 2, p. 193, 2015.

[20] G.-J.-A. H. Wetzelaer, M. Scheepers, A. M. Sempere, C. Momblona, J. Ávila, and H. J. Bolink, "Trap-assisted non-radiative recombination in organic-inorganic perovskite solar cells," *Adv. Mater.*, vol. 27, no. 11, pp. 1837–1841, Mar. 2015.

[21] T. Leijtens, G. E. Eperon, A. J. Barker, G. Grancini, W. Zhang, J. M. Ball, A. R. S. Kandada, H. J. Snaith, and A. Petrozza, "Carrier trapping and recombination: The role of defect physics in enhancing the open circuit voltage of metal halide perovskite solar cells," *Energy Environ. Sci.*, vol. 9, no. 11, pp. 3472–3481, 2016.

[22] E. Conwell and V. F. Weisskopf, "Theory of impurity scattering in semiconductors," *Phys. Rev.*, vol. 77, no. 3, p. 388, 1950.

[23] Y. Yuan and J. Huang, "Ion migration in organometal trihalide perovskite and its impact on photovoltaic efficiency and stability," *Accounts Chem. Res.*, vol. 49, no. 2, pp. 286–293, Feb. 2016.

[24] T. Jin, M. Akhtaruzzaman, and Y. Yamamoto, "Synthesis and performance of new organic dyes and functional fullerenes for organic solar cells," in *Nanomaterials for Sustainable Energy*. Washington, DC, USA: ACS Publications, 2015, pp. 193–236.

[25] S. D. Stranks, "Nonradiative losses in metal halide perovskites," *ACS Energy Lett.*, vol. 2, no. 7, pp. 1515–1525, Jul. 2017.

[26] F. W. Low, C. W. Lai, N. Asim, M. Akhtaruzzaman, M. Alghoul, S. K. Tiong, and N. Amin, "An investigation on titanium doping in reduced graphene oxide by RF magnetron sputtering for dye-sensitized solar cells," *Sol. Energy*, vol. 188, pp. 10–18, Aug. 2019.

[27] K. Tvingstedt, O. Malinkiewicz, A. Baumann, C. Deibel, H. J. Snaith, V. Dyakonov, and H. J. Bolink, "Radiative efficiency of lead iodide based perovskite solar cells," *Sci. Rep.*, vol. 4, no. 1, May 2015, Art. no. 6071.

[28] J. Kim, S.-H. Lee, J. H. Lee, and K.-H. Hong, "The role of intrinsic defects in methylammonium lead iodide perovskite," *J. Phys. Chem. Lett.*, vol. 5, no. 8, pp. 1312–1317, Apr. 2014.

[29] C. Ran, J. Xu, W. Gao, C. Huang, and S. Dou, "Defects in metal triiodide perovskite materials towards high-performance solar cells: Origin, impact, characterization, and engineering," *Chem. Soc. Rev.*, vol. 47, no. 12, pp. 4581–4610, 2018.

[30] W.-J. Yin, T. Shi, and Y. Yan, "Unusual defect physics in $CH_3NH_3PbI_3$ perovskite solar cell absorber," *Appl. Phys. Lett.*, vol. 104, no. 6, Feb. 2014, Art. no. 063903.

[31] M. L. Agiorgousis, Y.-Y. Sun, H. Zeng, and S. Zhang, "Strong covalency-induced recombination centers in perovskite solar cell material $CH_3NH_3PbI_3$," *J. Amer. Chem. Soc.*, vol. 136, no. 41, pp. 14570–14575, Oct. 2014.

[32] A. Walsh, D. O. Scanlon, S. Chen, X. G. Gong, and S.-H. Wei, "Self-regulation mechanism for charged point defects in hybrid halide perovskites," *Angew. Chem. Int. Ed.*, vol. 54, no. 6, pp. 1791–1794, Feb. 2015.

[33] C. Eames, J. M. Frost, P. R. F. Barnes, B. C. O'Regan, A. Walsh, and M. S. Islam, "Ionic transport in hybrid lead iodide perovskite solar cells," *Nature Commun.*, vol. 6, no. 1, p. 7497, Nov. 2015.

[34] A. Buin, P. Pietsch, J. Xu, O. Voznyy, A. H. Ip, R. Comin, and E. H. Sargent, "Materials processing routes to trap-free halide perovskites," *Nano Lett.*, vol. 14, no. 11, pp. 6281–6286, Nov. 2014.

[35] J. Xu, A. Buin, A. H. Ip, W. Li, O. Voznyy, R. Comin, M. Yuan, S. Jeon, Z. Ning, J. J. McDowell, P. Kanjanaboos, J.-P. Sun, X. Lan, L. N. Quan, D. H. Kim, I. G. Hill, P. Maksymovych, and E. H. Sargent, "Perovskite–fullerene hybrid materials suppress hysteresis in planar diodes," *Nature Commun.*, vol. 6, no. 1, p. 7081, Nov. 2015.

[36] F. Wang, S. Bai, W. Tress, A. Hagfeldt, and F. Gao, "Defects engineering for high-performance perovskite solar cells," *npj Flexible Electron.*, vol. 2, no. 1, p. 22, 2018.

[37] R. N. Hall, "Electron-hole recombination in germanium," *Phys. Rev.*, vol. 87, no. 2, p. 387, 1952.

[38] W. Shockley and W. T. Read, "Statistics of the recombination of electrons and holes," *Phys. Rev.*, vol. 87, pp. 835–842, Sep. 1952.

[39] M. S. Jamal, S. A. Shahahmadi, M. A. A. Wadi, P. Chelvanathan, N. Asim, H. Misran, M. I. Hossain, N. Amin, K. Sopian, and M. Akhtaruzzaman, "Effect of defect density and energy level mismatch on the performance of perovskite solar cells by numerical simulation," *Optik*, vol. 182, pp. 1204–1210, Apr. 2019.

[40] M. A. Green, *Solar Cells: Operating Principles, Technology, and System Applications*. Englewood Cliffs, NJ, USA: Prentice-Hall, 1982, p. 288.

[41] G. Xing, N. Mathews, S. S. Lim, N. Yantara, X. Liu, D. Sabba, M. Grätzel, S. Mhaisalkar, and T. C. Sum, "Low-temperature solution-processed wavelength-tunable perovskites for lasing," *Nature Mater.*, vol. 13, no. 5, p. 476, 2014.

[42] S. D. Stranks, V. M. Burlakov, T. Leijtens, J. M. Ball, A. Goriely, and H. J. Snaith, "Recombination kinetics in organic-inorganic perovskites: Excitons, free charge, and subgap states," *Phys. Rev. A, Gen. Phys.*, vol. 2, no. 3, Sep. 2014, Art. no. 034007.

[43] Y. Yamada, T. Nakamura, M. Endo, A. Wakamiya, and Y. Kanemitsu, "Photocarrier recombination dynamics in perovskite $CH_3NH_3PbI_3$ for solar cell applications," *J. Amer. Chem. Soc.*, vol. 136, no. 33, pp. 11610–11613, Aug. 2014.

[44] X. Wu, M. T. Trinh, D. Niesner, H. Zhu, Z. Norman, J. S. Owen, O. Yaffe, B. J. Kudisch, and X.-Y. Zhu, "Trap states in lead iodide perovskites," *J. Amer. Chem. Soc.*, vol. 137, no. 5, pp. 2089–2096, 2015.

[45] M. J. Simpson, B. Doughty, B. Yang, K. Xiao, and Y.-Z. Ma, "Imaging electronic trap states in perovskite thin films with combined fluorescence and femtosecond transient absorption microscopy," *J. Phys. Chem. Lett.*, vol. 7, no. 9, pp. 1725–1731, May 2016.

[46] D. W. de Quilettes, S. M. Vorpahl, S. D. Stranks, H. Nagaoka, G. E. Eperon, M. E. Ziffer, H. J. Snaith, and D. S. Ginger, "Impact of microstructure on local carrier lifetime in perovskite solar cells," *Science*, vol. 348, no. 6235, pp. 683–686, May 2015.

[47] M. Vrućinić, C. Matthiesen, A. Sadhanala, G. Divitini, S. Cacovich, S. E. Dutton, C. Ducati, M. Atatüre, H. Snaith, R. H. Friend, H. Sirringhaus, and F. Deschler, "Local versus long-range diffusion effects of photoexcited states on radiative recombination in organic–inorganic lead halide perovskites," *Adv. Sci.*, vol. 2, no. 9, Sep. 2015, Art. no. 1500136.

[48] D. Meggiolaro and F. De Angelis, "First-principles modeling of defects in lead halide perovskites: Best practices and open issues," *ACS Energy Lett.*, vol. 3, no. 9, pp. 2206–2222, Sep. 2018.

[49] Z. Li, J. Chen, H. Li, Q. Zhang, Z. Chen, X. Zheng, G. Fang, and Y. Hao, "A facilely synthesized 'spiro' hole-transporting material based on spiro [3.3] heptane-2, 6-dispirofluorene for efficient planar perovskite solar cells," *RSC Adv.*, vol. 7, no. 66, pp. 41903–41908, 2017.

[50] W. Li, P. Da, Y. Zhang, Y. Wang, X. Lin, X. Gong, and G. Zheng, "WO_3 nanoflakes for enhanced photoelectrochemical conversion," *ACS Nano*, vol. 8, no. 11, pp. 11770–11777, Nov. 2014.

[51] P. Schulz, E. Edri, S. Kirmayer, G. Hodes, D. Cahen, and A. Kahn, "Interface energetics in organo-metal halide perovskite-based photovoltaic cells," *Energy Environ. Sci.*, vol. 7, no. 4, pp. 1377–1381, Feb. 2014.

[52] C. C. Homes, "Optical response of high-dielectric-constant perovskite-related oxide," *Science*, vol. 293, no. 5530, pp. 673–676, Jul. 2001.

[53] G. Giorgi, J.-I. Fujisawa, H. Segawa, and K. Yamashita, "Small photocarrier effective masses featuring ambipolar transport in methylammonium lead iodide perovskite: A density functional analysis," *J. Phys. Chem. Lett.*, vol. 4, no. 24, pp. 4213–4216, Dec. 2013.

[54] C. Wehrenfennig, G. E. Eperon, M. B. Johnston, H. J. Snaith, and L. M. Herz, "High charge carrier mobilities and lifetimes in organolead trihalide perovskites," *Adv. Mater.*, vol. 26, no. 10, pp. 1584–1589, Mar. 2014.

[55] M. I. Hossain, F. H. Alharbi, and N. Tabet, "Copper oxide as inorganic hole transport material for lead halide perovskite based solar cells," *Sol. Energy*, vol. 120, pp. 370–380, Oct. 2015.

[56] N. Devi, K. A. Parrey, A. Aziz, and S. Datta, "Numerical simulations of perovskite thin-film solar cells using a CdS hole blocking layer," *J. Vac. Sci. Technol. B, Nanotechnol. Microelectron., Mater., Process., Meas., Phenomena*, vol. 36, no. 4, 2018, Art. no. 04G105.

[57] A. Hima, N. Lakhdar, B. Benhaoua, A. Saadoune, I. Kemerchou, and F. Rogti, "An optimized perovskite solar cell designs for high conversion efficiency," *Superlattices Microstruct.*, vol. 129, pp. 240–246, May 2019.

[58] J. M. Berak and M. J. Sienko, "Effect of oxygen-deficiency on electrical transport properties of tungsten trioxide crystals," *J. Solid State Chem.*, vol. 2, no. 1, pp. 109–133, Jun. 1970.

[59] T. Oku, "Crystal structures of $CH_3NH_3PbI_3$ and related perovskite compounds used for solar cells," *Sol. Cells-New Approaches Rev.*, vol. 1, 2015.

[60] M. Dongol, A. El-Denglawey, M. S. A. El Sadek, and I. S. Yahia, "Thermal annealing effect on the structural and the optical properties of nano CdTe films," *Optik*, vol. 126, no. 14, pp. 1352–1357, Jul. 2015.

[61] J. I. Langford and A. J. C. Wilson, "Scherrer after sixty years: A survey and some new results in the determination of crystallite size," *J. Appl. Crystallogr.*, vol. 11, no. 2, pp. 102–113, Apr. 1978.

[62] N. M. A. Rashid, C. Haw, W. Chiu, N. H. Khanis, A. Rohaizad, P. Khiew, and S. A. Rahman "Structural- and optical-properties analysis of single crystalline hematite (α-Fe_2O_3) nanocubes prepared by one-pot hydrothermal approach," *CrystEngComm*, vol. 18, no. 25, pp. 4720–4732, 2016.

[63] G. K. Williamson and R. E. Smallman, "III. Dislocation densities in some annealed and cold-worked metals from measurements on the X-ray debye-scherrer spectrum," *Philos. Mag.*, vol. 1, no. 1, pp. 34–46, 1956.

[64] A. D. Wright, C. Verdi, R. L. Milot, G. E. Eperon, M. A. Pérez-Osorio, H. J. Snaith, F. Giustino, M. B. Johnston, and L. M. Herz, "Electron–phonon coupling in hybrid lead halide perovskites," *Nature Commun.*, vol. 7, May 2016, Art. no. 11755.

[65] S. Rudin, T. L. Reinecke, and B. Segall, "Temperature-dependent exciton linewidths in semiconductors," *Phys. Rev. B, Condens. Matter*, vol. 42, no. 17, p. 11218, 1990.

[66] J. Lee, E. S. Koteles, and M. O. Vassell, "Luminescence linewidths of excitons in GaAs quantum wells below 150 K," *Phys. Rev. B, Condens. Matter*, vol. 33, no. 8, p. 5512, 1986.

[67] L. Malikova, W. Krystek, F. H. Pollak, N. Dai, A. Cavus, and M. C. Tamargo, "Temperature dependence of the direct gaps of ZnSe and $Zn_{0.56}$ $Cd_{0.44}$ Se," *Phys. Rev. B, Condens. Matter*, vol. 54, no. 3, p. 1819, 1996.

[68] A. K. Viswanath, J. I. Lee, D. Kim, C. R. Lee, and J. Y. Leem, "Exciton-phonon interactions, exciton binding energy, and their importance in the realization of room-temperature semiconductor lasers based on GaN," *Phys. Rev. B, Condens. Matter*, vol. 58, no. 24, p. 16333, 1998.